Synthesis and Crystal Structure of the High-pressure Cobalt Borate HP-CoB_2O_4

Stephanie C. Neumair[a], Reinhard Kaindl[b], and Hubert Huppertz[a]

[a] Institut für Allgemeine, Anorganische und Theoretische Chemie, Leopold-Franzens Universität Innsbruck, Innrain 52a, 6020 Innsbruck, Austria
[b] Institut für Mineralogie und Petrographie, Leopold-Franzens Universität Innsbruck, Innrain 52, 6020 Innsbruck, Austria

Reprint requests to H. Huppertz. E-mail: Hubert.Huppertz@uibk.ac.at

Z. Naturforsch. **2010**, *65b,* 1311 – 1317; received August 18, 2010

The cobalt borate HP-CoB_2O_4 was synthesized from Co_3O_4 and B_2O_3 under high-pressure / high-temperature conditions of 6.5 GPa and 950 °C. The structure of HP-CoB_2O_4 is isotypic to HP-NiB_2O_4 and β-FeB_2O_4, representing the third example of a borate, in which every BO_4 tetrahedron shares a common edge with a second one. HP-CoB_2O_4 crystallizes in the space group $C2/c$ ($Z = 4$) with the parameters $a = 934.6(2)$, $b = 562.0(2)$, $c = 443.3(1)$ pm, $\beta = 108.2(1)°$, $V = 0.2212(1)$ nm^3, $R_1 = 0.0218$, and $wR_2 = 0.0410$ (all data). The structure consists of layers of BO_4 tetrahedra, that are interconnected *via* strings of edge-sharing FeO_6 octahedra.

Key words: Borate, High Pressure, Crystal Structure, Multianvil

Introduction

In the last years, the efficient use of the multianvil high-pressure technique [1, 2] opened up new fields of synthesis, which were out of reach till then. Our research has been orientated into the investigation of borate chemistry under high-pressure / high-temperature conditions. Apart from the transformation of known borates to new high-pressure polymorphs (*e. g.* δ-BiB_3O_6 [3]), the syntheses led to compounds with new compositions and interesting structural features. The most striking discovery was the structural motif of edge-sharing BO_4 tetrahedra ($[B_2O_6]^{6-}$ units). For the first time, it was observed in 2002 in the rare-earth borate $Dy_4B_6O_{15}$ [4, 5] and two years later in the isotypic holmium phase $Ho_4B_6O_{15}$ [5, 6]. A second series of borates, which exhibit edge-sharing BO_4 tetrahedra in a different structure type, could be synthesized with the composition α-$RE_2B_4O_9$ (RE = Sm–Ho) [7 – 9]. In these examples, only $1/3$ ($RE_4B_6O_{15}$ (RE = Dy, Ho)) or $1/10$ (α-$RE_2B_4O_9$ (RE = Sm–Ho)) of the BO_4 tetrahedra bridge to a second tetrahedron *via* a common edge. In the last three years, we could synthesize two isotypic borates, in which all BO_4 tetrahedra share a common edge with a second tetrahedron: HP-NiB_2O_4 [10] and β-FeB_2O_4 [11]. Up to now, we cannot predict the occurrence of edge-sharing BO_4 tetrahedra. To our astonishment, the structural feature of edge-sharing BO_4 tetrahedra was recently found in the compound $KZnB_3O_6$, synthesized under ambient-pressure conditions [12, 13]. Thus, the structural motif of edge-sharing BO_4 tetrahedra is no longer a domain of high-pressure chemistry, but still favored under these conditions, as there are eleven different compounds with three structure types prepared under high-pressure, and only one compound synthesized under ambient-pressure conditions. In this context, we recently synthesized the compounds $M_6B_{22}O_{39} \cdot H_2O$ (M = Fe, Co) [14], which are built up from corner-sharing BO_4 tetrahedra, forming corrugated multiple layers, interconnected by BO_3 groups. The standard planar geometry of the BO_3 groups in these compounds is distorted, their structure being close to that of BO_4 tetrahedra if additional oxygen atoms of the neighboring BO_4 tetrahedra are considered to be part of the coordination sphere of the boron atoms. This situation can be regarded as an intermediate state on the way to edge-sharing tetrahedra.

A closer look at the system Co-B-O reveals the known compositions $Co_3(BO_3)_2$ [15], CoB_4O_7 [16], $Co_4B_6O_{13}$ [16], $Co_2B_2O_5$ [16, 17], and $Co_3(BO_3)O_2$ [18] under normal pressure conditions. In 2009, the first high-pressure cobalt borate β-CoB_4O_7 [19] was synthesized. With the synthesis of HP-CoB_2O_4 we

Table 1. Crystal data and structure refinement of HP-CoB_2O_4 (standard deviations in parentheses).

Empirical formula	HP-CoB_2O_4
Molar mass, g mol^{-1}	144.55
Crystal system	monoclinic
Space group	$C2/c$
Powder diffractometer	Stoe Stadi P
Radiation; λ, pm	Mo$K_{\alpha1}$; 70.93 (Ge(111) monochromator)
Powder data: a, pm	934.8(2)
b, pm	561.73(8)
c, pm	443.44(5)
β, deg	108.2(1)
V, nm^3	0.2212(1)
Single-crystal diffractometer	Nonius Kappa CCD
Radiation; λ, pm	MoK_α; 71.073 (graphite monochromator)
Single-crystal data: a, pm	934.6(2)
b, pm	562.0(2)
c, pm	443.3(1)
β, deg	108.2(1)
V, nm^3	0.2212(1)
Formula units per cell	$Z = 4$
Calculated density, g cm^{-3}	4.34
F(000), e	276
Crystal size, mm^3	0.08 × 0.04 × 0.04
Temperature, K	293(2)
Detector distance, mm	36
Exposure time, min	3.3
Absorption coefficient, mm^{-1}	7.5
Absorption correction	multi-scan (SCALEPACK [28])
θ range, deg	4.3 – 37.8
Range in hkl	±16, ±9, −7 / +6
Total no. of reflections	1832
Independent reflections / R_{int}	602 / 0.0279
Reflections with $I \geq 2\,\sigma(I)$ / R_σ	567 / 0.0286
Data / ref. parameters	602 / 33
Final indices R_1 / wR_2 [$I \geq 2\sigma(I)$]	0.0196 / 0.0403
Indices R_1 / wR_2 (all data)	0.0218 / 0.0410
Goodness-of-fit on F^2	1.096
Largest diff. peak / hole, e Å^{-3}	0.67 / −0.50

could now add a second high-pressure phase with a new composition to the ternary system Co-B-O, of which we report here the synthesis, crystal structure, and properties. Furthermore, similarities and differences to the isotypic compounds HP-NiB_2O_4 [10] and β-FeB_2O_4 [11] are discussed.

Experimental Section

Synthesis

The compound HP-CoB_2O_4 was synthesized under high-pressure high-temperature conditions of 6.5 GPa and 950 °C in a modified Walker-type multianvil apparatus. A stoichiometric mixture of Co_3O_4 (Fluka AG, Buchs, Switzerland, *p. a.*) and B_2O_3 (Strem Chemicals, Newburyport, USA, 99.9 %) (1 : 3) was ground together and filled into a boron nitride crucible (Henze BNP GmbH®, HeBoSint® S10, Kempten, Germany). This crucible was positioned into the center of an 18/11-assembly and compressed by eight tungsten carbide cubes (TSM-10, Ceratizit, Reutte, Austria). The pressure was applied *via* a Walker-type multianvil device and a 1000 t press (both devices from the company Voggenreiter, Mainleus, Germany). A detailed description of the assembly can be found in refs. [2, 20 – 23]. To synthesize HP-CoB_2O_4, the mixture was compressed to 6.5 GPa within three hours and kept at this pressure for the heating period. The temperature was increased in 10 min to 950 °C, kept there for 15 min, and decreased to 450 °C in 40 min. The sample was cooled down to r. t. by switching off the heating, followed by a decompression period of 9 h. The recovered pressure medium was broken apart, and the surrounding boron nitride crucible was removed from the sample. The compound HP-CoB_2O_4 was gained in form of violet crystals from a complex product mixture of at least three phases. Unfortunately, it was not possible to receive a phase-pure sample up to now. However, the corresponding reflections of HP-CoB_2O_4 in the powder pattern could be indexed (Table 1), and due to the characteristic color of HP-CoB_2O_4 it was possible to isolate single-crystals from the mixture for the structure determination and the spectroscopic investigations (IR/Raman).

Table 2. Atomic coordinates and isotropic equivalent displacement parameters U_{eq} (Å^2) for HP-CoB_2O_4 (space group: $C2/c$) (standard deviations in parentheses). U_{eq} is defined as one third of the trace of the orthogonalized U_{ij} tensor.

Atom	W. position	x	y	z	U_{eq}
Co	4e	1/2	0.84194(4)	1/4	0.0056(1)
B	8f	0.3132(2)	0.6073(2)	0.6242(3)	0.0049(2)
O1	8f	0.64442(9)	0.8480(2)	0.9778(2)	0.0050(2)
O2	8f	0.36098(9)	0.5872(2)	0.9661(2)	0.0050(2)

During the synthesis, the cobalt cations of Co_3O_4 with the oxidation state 3+ were reduced to the oxidation state 2+. A reduction of metal ions to lower oxidation states is often observed in the reducing environment of the multianvil high-pressure assembly, when hexagonal boron nitride is used as crucible material [24]. A precise explanation of the redox mechanism with hexagonal boron nitride as reducing agent can not yet be given.

FTIR spectroscopy

FTIR-ATR (*A*ttenuated *T*otal *R*eflection) spectra of single crystals were recorded with a Bruker Vertex 70 FT-IR spectrometer (spectral resolution 4 cm^{-1}) attached to a Hyperion 3000 microscope in a spectral range from 600 – 4000 cm^{-1}. A frustrum-shaped germanium ATR-crystal with a tip diameter of 100 μm was pressed onto the surface of the borate crystal with a power of 5 N, which crushed it into pieces of μm-size. 64 scans for the sample and the background were

Table 3. Anisotropic displacement parameters U_{ij} (Å^2) for HP-CoB_2O_4 (space group: $C2/c$) (standard deviations in parentheses).

Atom	U_{11}	U_{22}	U_{33}	U_{23}	U_{13}	U_{12}
Co	0.0056(2)	0.060(2)	0.0057(2)	0	0.00253(7)	0
B	0.0054(4)	0.0048(4)	0.0046(5)	0.0000(4)	0.0016(4)	0.0001(4)
O1	0.0046(3)	0.0051(3)	0.0055(3)	−0.0003(2)	0.0017(3)	0.0003(2)
O2	0.0058(3)	0.0056(3)	0.0036(3)	0.0001(3)	0.0014(3)	−0.0010(2)

acquired. Beside the correction of the spectra for atmospheric influences, an enhanced ATR correction [25], using the OPUS 6.5 software, was performed. A mean refraction index of the sample of 1.6 was assumed for the ATR correction. Background correction and peak fitting were carried out *via* polynomial and folded Gaussian-Lorentzian functions.

Raman spectroscopy

The confocal Raman spectra of the single crystals in the range 100 – 4000 cm^{-1} were obtained with a Horiba Jobin Yvon LabRam-HR 800 Raman micro-spectrometer. The sample was excited by the 532 nm emission line of a 30 mW Nd-YAG-laser under an Olympus 100× objective (numerical aperture = 0.9). The size and power of the laser spot on the surface were approximately 1 μm and 5 mW, respectively. The scattered light was dispersed by a grating with 1800 lines mm^{-1} and collected by a 1024 × 256 open electrode CCD detector. The spectral resolution, determined by measuring the Rayleigh line, was about 1.4 cm^{-1}. Polynomial and convoluted Gauss-Lorentz functions were applied for background correction and band fitting. The wavenumber accuracy of about 0.5 cm^{-1} was achieved by adjusting the zero-order position of the grating and regularly checked by a Neon spectral calibration lamp.

Crystal structure analysis

The powder diffraction pattern was obtained in transmission geometry, using a Stoe Stadi P powder diffractometer with monochromatized Mo$K_{\alpha 1}$ (λ = 70.93 pm) radiation. It was indexed with the program ITO [26] on the basis of a monoclinic unit cell. The lattice parameters (Table 1) were calculated from least-squares fits of the powder data. The correct indexing of the pattern of HP-CoB_2O_4 was confirmed by intensity calculations, taking the atomic positions from the structure refinement [27].

For the single-crystal structure analysis, small irregularly shaped crystals of HP-CoB_2O_4 were isolated by mechanical fragmentation. Measurements of the single-crystal intensity data were carried out at r. t. with a Nonius Kappa CCD 4-circle diffractometer, equipped with graphite-monochromatized MoK_α (λ = 71.073 pm) radiation, a Micracol Fiber Optics collimator, and a Nonius FR590 generator. A semiempirical absorption correction, based on equivalent and redundant intensities (SCALEPACK [28]), was applied to the intensity data. The positional parameters of the isotypic compound β-FeB_2O_4 were used as starting values for the structure refinement of HP-CoB_2O_4 (SHELXL-97 [29, 30]). All atoms were refined with anisotropic displacement parameters. Final difference Fourier syntheses did not reveal any significant peaks in the refinements. All relevant details of the data collections and evaluations are listed in Table 1. Furthermore, the Tables 2 – 4 show the positional parameters, the anisotropic thermal displacement parameters, selected interatomic distances, and angles.

Table 4. Interatomic distances (pm) and angles (deg) for HP-CoB_2O_4 (space group: $C2/c$), based on single-crystal data (standard deviations in parentheses).

Co–O2 (2×)	207.4(2)	B–O2a	144.2(2)
Co–O1b (2×)	207.3(2)	B–O2b	144.4(2)
Co–O1a (2×)	224.2(1)	B–O1a	151.7(2)
	av. = 213.0	B–O1b	152.8(2)
			av. = 148.3
O2a–Co–O2b	92.69(5)	B–O1–B	86.71(8)
O2a–Co–O1a	93.23(3)	B–O2–B	122.36(9)
O2b–Co–O1a	88.07(3)		av. = 104.5
O2a–Co–O1b	88.07(3)		
O2b–Co–O1b	93.23(3)	O2a–B–O2b	114.19(9)
O2b–Co–O1c	95.06(4)	O2a–B–O1b	112.42(9)
O1a–Co–O1c	80.77(3)	O2b–B–O1a	111.00(9)
O1b–Co–O1c	97.76(3)	O2a–B–O1a	111.69(9)
O2a–Co–O1d	95.06(4)	O2b–B–O1b	113.48(9)
O1a–Co–O1d	97.76(3)	O1a–B–O1b	93.29(8)
O1b–Co–O1d	80.77(3)		av. = 109.3
O1c–Co–O1d	77.98(2)		
	av. = 90.1		

Further details of the crystal structure investigation may be obtained from Fachinformationszentrum Karlsruhe, 76344 Eggenstein-Leopoldshafen, Germany (fax: +49-7247-808-666; e-mail: crysdata@fiz-karlsruhe.de, http://www.fiz-informationsdienste.de/en/DB/icsd/depot_anforderung.html) on quoting the deposition number CSD-422063.

Results and Discussion

The crystal structure of HP-CoB_2O_4 is depicted in Fig. 1 with a view along [00$\bar{1}$]. This centrosymmetric oxoborate is composed of layers of distorted BO_4 tetrahedra in the *bc* plane. These layers are linked by strings of edge-sharing CoO_6 octahedra, running along the *c* direction. Fig. 2 shows that inside the layers each of the BO_4 tetrahedra is connected to a second one *via* edge-sharing, forming B_2O_6 units. These units are interconnected *via* common corners, resulting in "sechser" rings [31] formed by four B_2O_6 units. For a

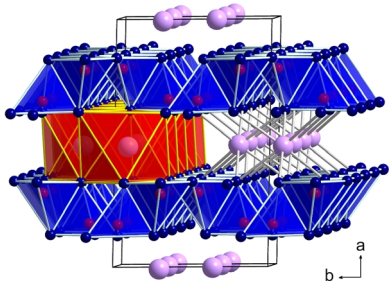

Fig. 1 (color online). Crystal structure of HP-CoB_2O_4 as viewed along [00$\bar{1}$]. Blue polyhedra (top and bottom layer): BO_4 tetrahedra; red polyhedra (center layer): CoO_6 octahedra, violet spheres (large): Co^{2+}; blue spheres (corners of tetrahedra): O^{2-}; red spheres (centers of tetrahedra): B^{3+}.

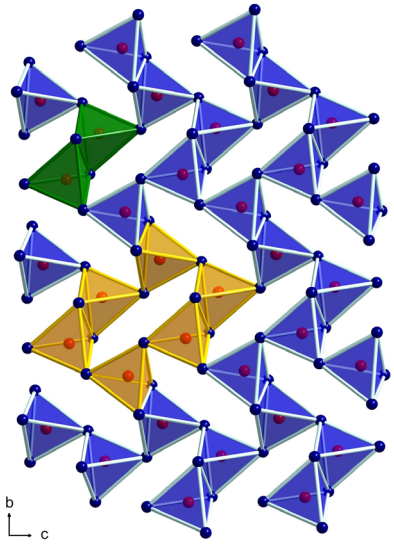

Fig. 2 (color online). Layer of edge-sharing BO_4 tetrahedra in HP-CoB_2O_4, viewed along [100]. One B_2O_6 unit is highlighted dark green; one "sechser" ring highlighted in light yellow.

more detailed description of the HP-NiB_2O_4 structure type see ref. [10].

As already mentioned, the structure of HP-CoB_2O_4 is isotypic to HP-NiB_2O_4 [10] and β-FeB_2O_4 [11]. Unfortunately, the designation (prefix) is not identical. When the first isotype (HP-NiB_2O_4) was synthesized under high-pressure conditions, we designated this compound with the prefix HP (*H*igh *P*ressure), because up to now, there exists no ambient-pressure phase of the composition NiB_2O_4. The same is true for HP-CoB_2O_4. In contrast, when β-FeB_2O_4 was synthesized, there already existed the iron borate α-FeB_2O_4 [32], synthesized also under high-pressure conditions.

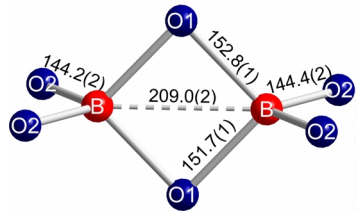

Fig. 3 (color online). The B_2O_6 unit in HP-CoB_2O_4 and selected bond lengths (pm).

Thus, the second high-pressure iron borate got the prefix β to distinguish these two polymorphs.

Fig. 3 shows selected interatomic angles and distances inside the B_2O_6 unit of HP-CoB_2O_4. As expected, the B–O distances inside the B_2O_2 ring (B1–O1: 151.7(2) pm, 152.8(2) pm) are longer than those outside the "zweier" rings [31] (B1–O2: 144.2(2) pm, 144.4(2)). The average B–O bond length of 148.3 pm is slightly increased in comparison to the average distance of 147.6 pm in BO_4 tetrahedra [33, 34]. Inside the B_2O_6 unit, the B···B distance comes to 209.0(2) pm, which fits well with values found in other high-pressure borates with edge-sharing BO_4 tetrahedra, *e. g.* β-FeB_2O_4 (208.3(5) pm) [11], HP-NiB_2O_4 (208.8(2) pm) [10], α-$RE_2B_4O_9$ (RE = Sm: 207.1(9) pm; Eu: 205.3(9) pm; Gd: 204(2) pm; Tb: 205.5(9); Ho: 204(3) pm) [7]–[9], $RE_4B_6O_{15}$ (RE = Dy: 207.2(8) pm, Ho: 207(1) pm) [4–6], and $KZnB_3O_6$ (207.9(4) pm) [12, 13].

In the distorted CoO_6 octahedra, the Co–O distances vary between 207.3(2) and 224.20(9) pm and average to 213.0 pm. This value is in good agreement with the average Co^{2+}–O bond lengths in CoO_6 octahedra of 212.2 pm found in $Co_2B_2O_5$ [16, 17].

Furthermore, bond-valence sums were calculated for all atoms of HP-CoB_2O_4, using the bond-length/bond-strength concept (ΣV) [35, 36] and the CHARDI concept (*Char*ge *Di*stribution in Solids, ΣQ) [37]. The results of both concepts confirm the supposed formal ionic charges, deduced from the crystal structure (ΣV: +1.88 (Co), +2.97 (B), −1.91 (O1), −2.00 (O2) and ΣQ: +2.04 (Co), +2.98 (B), −1.87 (O1), −2.13 (O2)).

The MAPLE values (*Ma*delung *P*art of *L*attice *E*nergy) [38–40] were calculated in order to compare them with the data of the binary component CoO and the high-pressure modification B_2O_3-II. Due to the additive potential of the MAPLE values, it is possible to calculate hypothetical values for HP-CoB_2O_4, starting

Table 5. Comparison of the isotypic structures of β-FeB_2O_4 [11], HP-CoB_2O_4, and HP-NiB_2O_4 [10].

Empirical formula	β-FeB_2O_4	HP-CoB_2O_4	HP-NiB_2O_4
Molar mass, g mol^{-1}	141.5	144.6	144.3
Crystal system		— monoclinic —	
Space group		— $C2/c$ —	
Unit cell dimensions:			
a, pm	950.0(2)	934.6(2)	924.7(2)
b, pm	562.9(2)	562.0(2)	552.3(2)
c, pm	443.7(1)	443.3(1)	442.9(1)
β, deg	108.5(1)	108.2(1)	108.3(1)
V, nm^3	0.225(1)	0.221(1)	0.215(1)
B–O bond lengths, pm:			
B–O1	151.2(4)	151.7(2)	151.6(2)
	152.5(4)	152.8(2)	153.1(2)
B–O2	144.3(4)	144.4(2)	144.5(2)
	144.3(4)	144.2(2)	144.3(2)
av. B–O distance, pm	148.1	148.3	148.4
B···B distance in the B_2O_6 unit, pm	208.3(5)	209.0(2)	208.8(2)
av. M–O distance, pm	215.3	213.0	208.6
$r(M^{2+})$, pm [43, 44]	92 (hs), 75 (ls)	89 (hs), 79 (ls)	83

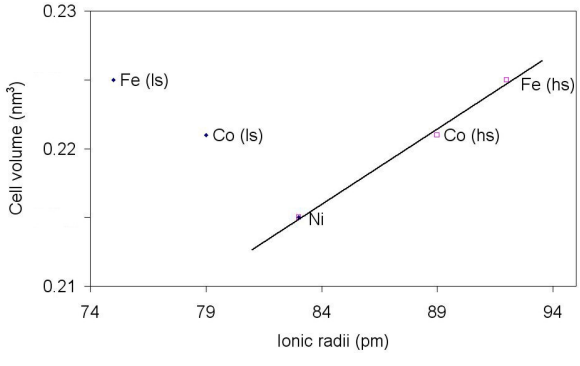

Fig. 4 (color online). Illustration of the correlation of the unit cell volume and the ionic radii of β-FeB_2O_4 [11], HP-CoB_2O_4, and HP-NiB_2O_4 for the high-spin (hs, □) and the low-spin (ls, ◆) state.

from the binary oxides. A value of 26297 kJ mol^{-1} was obtained, which is to be compared to 26498 kJ mol^{-1} (deviation = 0.8 %) for the binary oxides {1 × CoO (4560 kJ mol^{-1}) [41] + 1 × B_2O_3-II (21938 kJ mol^{-1}) [42]}.

In spite of the isotypy, there are differences in the structures, owing to the variation of the ionic radii and the electronic configuration of the metal ions. Table 5 lists the different ionic radii [43, 44]. For Fe^{2+} and Co^{2+}, both the high-spin (hs) and the low-spin (ls) states are listed for a comparison of selected structural parameters of the isotypic structures β-FeB_2O_4 and HP-MB_2O_4 (M = Co, Ni). Fig. 4 shows a graph of the coherence of the increasing cell volume with the larger ionic radii of Co^{2+}(hs) and Fe^{2+}(hs). The unit cell volumes of the compounds show a positive linear gradient only with the ionic radii of the metal cations in their high-spin state. The low-spin states of Fe^{2+} and Co^{2+} would imply an increase of the cell volume with decreasing ionic radii of Fe^{2+} and Co^{2+}, which would be anomalous. A closer look at the lattice parameters b and c (Table 5) reveals only a minor or rather no difference. In contrast, the lattice parameter a shows remarkable differences (β-FeB_2O_4: 950.0(2) pm, HP-CoB_2O_4: 934.6(2) pm, HP-NiB_2O_4: 924.7(2) pm). Due to the fact that the differences in bond lengths and angles within the BO_4 tetrahedra of the three compounds are negligible, the reason for the different lattice parameter has to be found in the ionic radii of the cations. Compared to HP-CoB_2O_4, the increased ionic radius of Fe^{2+} (hs) leads to an enlargement of the interlayer distance in β-FeB_2O_4 along a and a broadening of the strings of the FeO_6 octahedra along b. In the c direction, no elongation of the strings of octahedra can be observed. In HP-NiB_2O_4, the decreased ionic radius of Ni^{2+} causes a shortening of the interlayer distance along a and of the strings of NiO_6 octahedra along b.

Vibrational spectroscopy

The FTIR-ATR and Raman spectra of HP-CoB_2O_4 are displayed in Figs. 5 and 6, respectively. Assignments of the vibrational modes are based on a comparison with the experimental data of borate glasses and crystals containing BO_3 and BO_4 building units

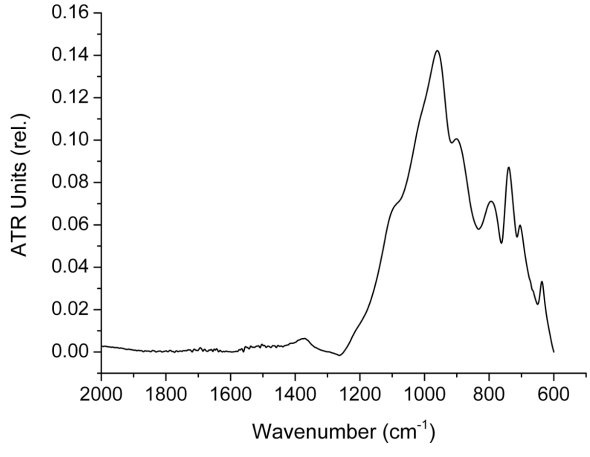

Fig. 5. FTIR-ATR (*A*ttenuated *T*otal *R*eflection) spectrum of a HP-CoB_2O_4 single crystal in the range 2000 – 600 cm^{-1}.

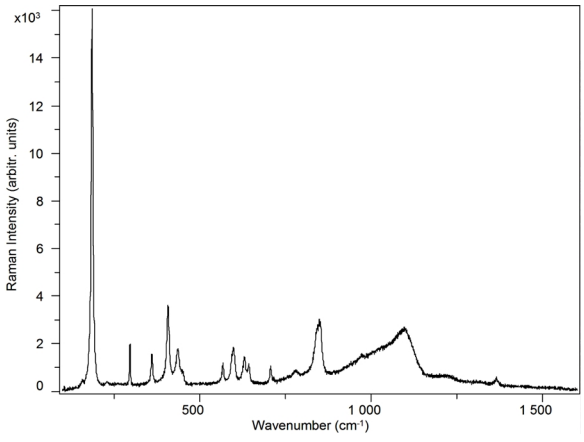

Fig. 6. Raman spectrum of HP-CoB_2O_4.

[34, 45 – 49]. In the IR-absorption spectrum, several groups of bands were detected around 650 and between 700 and 850, together with a strong band around 1000 and a weak band at 1380 cm^{-1}. The Raman spectrum of HP-CoB_2O_4 is characterized by the most intense line at 187 cm^{-1} and several groups of lines around 400, 600, 850, and 1100 – 1400 cm^{-1}.

Vibrational spectra of borate compounds containing edge-sharing B_2O_6 units were reported in refs. [11, 14, 16]. The authors assigned bands in the region 800 – 1100 cm^{-1} to stretching modes of units with boron tetrahedrally coordinated to oxygen. The antisymmetric stretching modes are expected to be intense in the IR spectrum and located around 1050 cm^{-1}, and the Raman-active symmetric stretching modes between 850 and 900 cm^{-1} [50]. Absorption bands and Raman lines between 1200 and 1450 cm^{-1} would be expected for oxoborates containing BO_3 groups, which do not occur in the structure of HP-CoB_2O_4. The Raman spectrum exhibits weak lines at 1200 and 1360 cm^{-1}, which were shown to be presumably related to symmetrical stretching modes of edge-sharing BO_4 tetrahedra in the B_2O_6 units in refs. [11, 14, 16]. However, these lines are weaker and occur at decreased wavenumbers compared to those of HP-NiB_2O_4 (1262 and 1444 cm^{-1} [10]). Bands below 800 cm^{-1} can be assigned to complex bending and stretching vibrations of the B_2O_6 unit, Co–O bonds, and lattice vibrations. In the range from 2000 to 4000 cm^{-1}, where vibrational modes caused by OH groups or water molecules contained in the structure are expected, only bands caused by nail finish contamination or adsorbed water could be detected.

Conclusions

In this paper, the synthesis and crystal structure of the high-pressure phase HP-CoB_2O_4 is reported and compared to the isotypic phases β-FeB_2O_4 and HP-NiB_2O_4. The structure consists of layers of BO_4 tetrahedra connected *via* strings of edge-sharing CoO_6 octahedra. The metal cations in β-FeB_2O_4 and HP-MB_2O_4 (M = Co, Ni) exist in the high-spin configuration.

Acknowledgements

We thank Dr. G. Heymann for collecting the single-crystal data. This work was financially supported by the Deutsche Forschungsgemeinschaft (HU 966/2-3) and the Fonds der Chemischen Industrie.

[1] H. Huppertz, *Chem. Commun.*, DOI:10.1039/C0CC02715D.
[2] H. Huppertz, *Z. Kristallogr.* **2004**, *219*, 330.
[3] J. S. Knyrim, P. Becker, D. Johrendt, H. Huppertz, *Angew. Chem.* **2006**, *118*, 8419; *Angew. Chem. Int. Ed.* **2006**, *45*, 8239.
[4] H. Huppertz, B. von der Eltz, *J. Am. Chem. Soc.* **2002**, *124*, 9376.
[5] H. Huppertz, *Z. Naturforsch.* **2003**, *58b*, 278.
[6] H. Huppertz, H. Emme, *J. Phys.: Condens. Matter* **2004**, *16,* 1283.
[7] H. Emme, H. Huppertz, *Z. Anorg. Allg. Chem.* **2002**, *628*, 2165.
[8] H. Emme, H. Huppertz, *Chem. Eur. J.* **2003**, *9*, 3623.
[9] H. Emme, H. Huppertz, *Acta Crystallogr.* **2005**, *C61*, i29.
[10] J. S. Knyrim, F. Roeßner, S. Jakob, D. Johrendt, I. Kinski, R. Glaum, H. Huppertz, *Angew.Chem.* **2007**, *119*, 9256; *Angew. Chem. Int. Ed.* **2007**, *46*, 9097.
[11] S. C. Neumair, R. Glaum, H. Huppertz, *Z. Naturforsch.* **2009**, *64b*, 883.
[12] Y. Wu, J.-Y. Yao, J.-X. Zhang, P.-Z. Fu, Y.-C. Wu, *Acta Crystallogr.* **2010**, *E66*, i45.
[13] S. Jin, G. Cai, W. Wang, M. He, S. Wang, X. Chen, *Angew. Chem.* **2010**, *122*, 5087; *Angew. Chem. Int. Ed.* **2010**, *49*, 4967.
[14] S. C. Neumair, J. S. Knyrim, O. Oeckler, R. Glaum, R. Kaindl, R. Stalder, H. Huppertz, *Chem. Eur. J.* **2010**, *16*, DOI:10.1002/chem.201001611.
[15] H. Effenberger, F. Pertlik, *Z. Kristallogr.* **1984**, *166*, 129.

[16] J. L. C. Rowsell, N. J. Taylor, L. F. Nazar, *J. Solid State Chem.* **2003**, *174*, 189.
[17] S. V. Berger, *Acta Chem. Scand.* **1950**, *4*, 1054.
[18] R. Norrestam, K. Nielsen, I. Sotofte, N. Thorup, *Z. Kristallogr.* **1989**, *189*, 33.
[19] S. C. Neumair, J. S. Knyrim, R. Glaum, H. Huppertz, *Z. Anorg. Allg. Chem*. **2009**, *635*, 2002.
[20] N. Kawai, S. Endo, *Rev. Sci. Instrum.* **1970**, *41,* 1178.
[21] D. Walker, M. A. Carpenter, C. M. Hitch, *Am. Mineral.* **1990**, *75*, 1020.
[22] D. Walker, *Am. Mineral.* **1991**, *76*, 1092.
[23] D. C. Rubie, *Phase Transitions* **1999**, *68*, 431.
[24] J. S. Knyrim, J. Friedrichs, S. Neumair, F. Roeßner, Y. Floredo, S. Jakob, D. Johrendt, R. Glaum, H. Huppertz, *Solid State Sci*. **2008**, *10*, 168.
[25] F. M. Mirabella, Jr. in *Internal Reflection Spectroscopy, Theory and Applications* (Ed.: F. M. Mirabella, Jr.), Marcel Dekker, New York, **1993**, p. 17.
[26] J. W. Visser, *J. Appl. Crystallogr*. **1969**, *2*, 89.
[27] WinXPOW (version 1.2), Stoe & Cie GmbH, Darmstadt (Germany) **2001**.
[28] Z. Otwinowski, W. Minor in *Methods in Enzymology*, Vol. 276, *Macromolecular Crystallography*, Part A (Eds.: C. W. Carter Jr., R. M. Sweet), Academic Press, New York, **1997**, pp. 307.
[29] G. M. Sheldrick, SHELXL-97, Program for the Refinement of Crystal Structures, University of Göttingen, Göttingen (Germany) **1997**.
[30] G. M. Sheldrick, *Acta Crystallogr*. **2008**, *A64*, 112.
[31] The term "sechser" ring was coined by F. Liebau (*Structural Chemistry of Silicates*, Springer, Berlin, **1985**) and is derived from the german word "sechs", which means six. However, a "sechser" ring is not a six-membered ring, but rather a ring with six tetrahedral centers (B) and six electronegative atoms (O). Similar terms exist for rings made up of two or three tetrahedral centers, namely "zweier" and "dreier" rings.
[32] J. S. Knyrim, H. Huppertz, *J. Solid State Chem*. **2008**, *181*, 2092.
[33] E. Zobetz, *Z. Kristallogr*. **1990**, *191*, 45.
[34] F. C. Hawthorne, P. C. Burns, J. D. Grice in *Reviews in Mineralogy*, Vol. 33, *Boron: Mineralogy, Petrology and Geochemistry* (Eds.: E. S. Grew, L. M. Anovitz), Mineralogical Society of America, Washington D. C. **1996**, p. 41.
[35] I. D. Brown, D. Altermatt, *Acta Crystallogr.* **1985**, *B41*, 244.
[36] N. E. Brese, M. O'Keeffe, *Acta Crystallogr.* **1991**, *B47*, 192.
[37] R. Hoppe, S. Voigt, H. Glaum, J. Kissel, H. P. Müller, K. J. Bernet, *J. Less-Common Met.* **1989**, *156*, 105.
[38] R. Hoppe, *Angew. Chem.* **1966**, *78*, 52; *Angew. Chem. Int. Ed.* **1966**, *5*, 95.
[39] R. Hoppe, *Angew. Chem.* **1970**, *82*, 7; *Angew. Chem. Int. Ed.* **1970**, *9*, 25.
[40] R. Hübenthal, M. Serafin, R. Hoppe, MAPLE (version 4.0), Program for the Calculation of Distances, Angles, Effective Coordination Numbers, Coordination Spheres, and Lattice Energies, University of Giessen, Giessen (Germany) **1993**.
[41] N. C. Tombs, H. P. Rooksby, *Nature* **1950**, *165*, 442.
[42] C. T. Prewitt, R. D. Shannon, *Acta Crystallogr.* **1968**, *B24*, 869.
[43] R. D. Shannon, C. T. Prewitt, *Acta Crystallogr.* **1969**, *B25*, 925.
[44] R. D. Shannon, *Acta Crystallogr.* **1976**, *A32*, 751.
[45] H. Huppertz, *J. Solid State Chem*. **2004**, *177*, 3700.
[46] G. Chadeyron, M. El-Ghozzi, R. Mahiou, A. Arbus, J. C. Cousseins, *J. Solid State Chem.* **1997**, *128*, 261.
[47] L. Jun, X. Shuping, G. Shiyang, *Spectrochim. Acta* **1995**, *A51*, 519.
[48] G. Padmaja, P. Kistaiah, *J. Phys. Chem.* **2009**, *A113*, 2397.
[49] J. C. Zhang, Y. H. Wang, X. Guo, *J. Lumin.* **2007**, *122-123*, 980.
[50] S. D. Ross, *Spectrochim. Acta* **1972**, *A28*, 1555.